

# Optimization Analysis of Interface Circuits in Piezoelectric Energy Harvesting Systems

Shuai Pang, Wenbin Li\*, Jiangming Kan

*School of Technology, Beijing Forestry University, Beijing, 100083, China*

## Abstract

Piezoelectric energy harvesting systems have different interface circuits, including the standard interface circuit, synchronized switch harvesting on inductor circuit, and synchronized charge extraction circuit. The comparison of an interface circuit with a different interface circuit to determine which is better has been widely investigated. However, for a certain interface circuit, how the parameters can be optimized to increase efficiency in energy collection has rarely been investigated. To improve the energy harvesting efficiency of a certain interface circuit in a fast and convenient manner, three interface circuits, which are the circuits to be optimized, were mainly introduced. A simulation method to optimize the circuit for energy collection was used. The simulation method was implemented in Pspice and includes parametric, sensitivity, and optimization analyses. The output power of parallel synchronized switch harvesting on the inductor circuit can be increased from 20.13 mW to 25.23 mW, and the output power of the synchronized charge extraction circuit can be increased from 11.98 mW to 19.85 mW. Results show that the energy collection performance can be improved by using the optimization simulation method.

**Keywords:** optimization, piezoelectric energy harvesting, interface circuit

## 1. Introduction

Transforming ambient energy from a living environment, transportation systems, or human bodies into electrical energy to supply low-power electronic devices has been extensively investigated in recent years [1–4]. Self-powered piezoelectric vibration energy harvesting techniques, which present a potentially sufficient power density, have received particular attention [5, 6]. A self-powered piezoelectric vibration energy harvesting system is usually composed of a mechanical oscillating structure, a piezoelectric electrical generator (PEG), an electrical interface circuit that converts the generated AC current into DC current, and an energy storage device that accumulates and stores energy for intermittent use [7, 8]. PEG has an oscillatory mechanical structure because of transduction principles. PEG is excited at its resonant frequency in many studies to generate the

maximum electrical energy. The output power will decrease if PEG is not excited at its resonant frequency. This problem can be solved by tuning the resonant frequency of PEG to match that of the mechanical oscillating structure or by widening the bandwidth of PEG. Recent studies that consider piezoelectric structures focused on developing wideband mechanical oscillators to enlarge PEG bandwidth [9, 10].

Apart from optimizing piezoelectric structures, electrical interface circuits also play an important role in increasing the harvested power of the system [11]. The standard interface circuit only involves a diode bridge rectifier and a smooth capacitor [12]. The synchronized switch harvesting on inductor (SSHI) circuit and the synchronized charge extraction (SCE) circuit have been proposed and improved to further increase the energy harvesting efficiency [13–17]. Different interface circuits have different characteristics. The simplified equivalent relation between the piezoelectric mechanical structure and the electrical circuit has been provided. Circuit models and parameters have been

\*Corresponding author

Email address: leewb@bjfu.edu.cn (Wenbin Li)

provided in several studies, but only a few studies have investigated parameter optimization to obtain high harvested power for a certain interface circuit. Thus, how the circuit can be optimized from the aspect of simulation is demonstrated in this study.

This paper is organized as follows. In Section 2, energy harvesting principles are introduced briefly. In Section 3, three types of interface circuits, namely, parallel-SSHI, series-SSHI, and SCE interface circuits, are analyzed using the method proposed in this study. In Section 4, the results are compiled in terms of the performance of the circuits. The conclusions are summarized in Section 5.

## 2. Energy Harvesting Principles

### 2.1. Single-degree-of-freedom system with cantilevered piezoelectric structure

Several types of mechanical structures exist. In this paper, the working principle and details of different PEGs are not described in detail. We regard the most investigated cantilevered piezoelectric structure as an example. Excited by a sinusoidal force at the resonant frequency, the energy harvesting structure can be modeled as a single-degree-of-freedom (SDOF) spring-mass-damper system [17–19]. Figure 1 shows the SDOF schematic representation of a base excited piezoelectric structure, where  $M$ ,  $C$ , and  $K$  respectively represent the equivalent mass, mechanical damping, and model stiffness, respectively.  $y(t)$  is the base displacement, and  $x(t)$  is the relative displacement of the structure motion.  $i_o$  is the current flowing out of the piezoelectric element, and  $v_p$  is the voltage across the piezoelectric element. Several studies discussed energy harvesting under broadband stochastic excitation [20, 21], but this study only considers the harmonically excited case, i.e.,  $\ddot{y}(t)$  is sinusoidal. The equation of motion for the system is provided by Eq. (1) [18, 19].

$$\begin{aligned} M\ddot{x}(t) + C\dot{x}(t) + Kx(t) \\ = F - \alpha v_p \\ = -M\ddot{y}(t) - \alpha v_p \end{aligned} \quad (1)$$

where:  $F$  is the excitation,  $\alpha$  is the force-voltage factor of the piezoelectric element.

The output current of the piezoelectric element  $i_o$ , as shown in Fig. 1 and Fig. 2, is provided by Eq. (2) [18, 19], and  $C_p$  is the clamped capacitor of the piezoelectric element as shown in Figure 2.

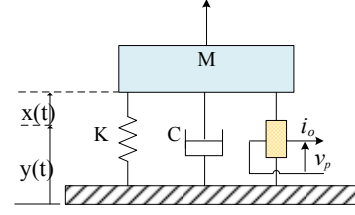


Figure 1: SDOF schematic representation of a base excited piezoelectric structure [18, 19]

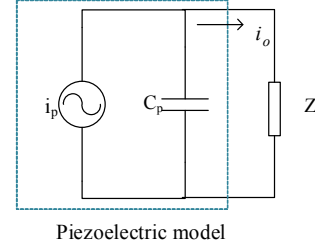


Figure 2: Equivalent block diagram of the piezoelectric element [22]

$$i_o = \alpha \dot{x}(t) - C_p \dot{v}_p \quad (2)$$

Eqs. (3) to (5) define  $C_p$ ,  $\alpha$ , and  $K$  in short circuit [17]. Ignoring the structure stiffness, the model stiffness  $K$  can be equal to the stiffness of the piezoelectric element in short circuit.  $A$  and  $H$  are the cross-section area and thickness of the piezoelectric element, respectively.  $\epsilon_{33}^S$  is a coefficient in the permittivity matrix,  $e_{33}$  is a coefficient in the piezoelectric stress matrix, and  $c_{33}^E$  is a coefficient in the elastic stiffness matrix.

$$C_p = \frac{\epsilon_{33}^S A}{H} \quad (3)$$

$$\alpha = \frac{e_{33} A}{H} \quad (4)$$

$$K = \frac{c_{33}^E A}{H} \quad (5)$$

A vibrating piezoelectric element is modeled as sinusoidal current  $i_p$  in parallel with capacitor  $C_p$ , as shown in Fig. 2 [12, 22].  $Z$  is the equivalent impedance.  $I_p$  is the magnitude of  $i_p$ , which varies with the mechanical excitation level of the piezoelectric element but is assumed to be relatively constant regardless of external loading. The equivalent current  $i_p$  is provided by Eq. (6) [18].

$$i_p = I_p \sin(\omega t) \quad (6)$$

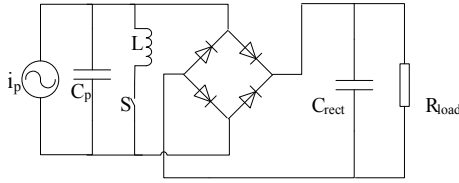


Figure 3: Standard interface circuit

where:  $\omega = 2\pi f$  is the excitation angular frequency of PEG and  $f$  is the excitation frequency of PEG. The magnitude of open-circuit voltage  $V_p$  is provided by Eq. (7) [18].

$$V_p = \frac{I_p}{\omega C_p} = \frac{\alpha X}{C_p} \quad (7)$$

where  $X$  is the magnitude of the relative displacement.

### 2.2. Interface circuits for piezoelectric energy harvesting

Several types of interface circuits exist for the collection and storage of piezoelectric energy. These interface circuits include the standard interface circuit shown in Fig. 3, the SSHI interface circuit shown in Fig. 4, and the SCE interface circuit shown in Fig. 5.  $S$  represents the switch and  $L$  is the inductor.  $C_{rect}$  is the filter and storage capacitor and  $R_{load}$  represents the load resistance. Further information on the working principles can be found in [11, 19, 22, 23]. Circuits for extreme displacement detection and switch control are required to implement the self-powered nonlinear SSHI and SCE interface circuits. The electronic breaker circuit for switching on maxima is shown in Fig. 6; it consists of an envelope detector, a comparator, and a digital switch. Minima switch control topology is conducted in a similar mode, with opposite polarities of diodes and transistors, as shown in Fig. 6.

### 3. Methodology

The previous sections provided the theoretical basis for the simulation analysis. In the simulation analysis,  $i_p$  and  $C_p$  were set first. OrCAD Cadence/PSpice 16.3 provided the simulation tools. Simulation analysis helps save time and cost in optimizing circuit designs.

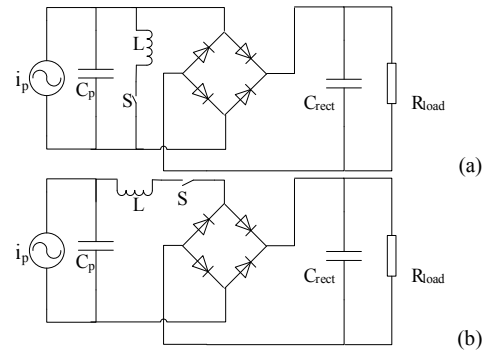


Figure 4: (a) Parallel-SSHI interface circuit, (b) Series-SSHI interface circuit

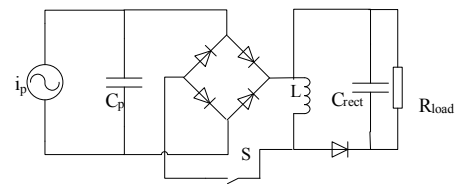


Figure 5: SCE interface circuit

The method of optimizing the circuit using OrCAD Cadence/PSpice is introduced in this section.

The interface circuits included the standard interface circuit, SSHI interface circuit, and SCE interface circuit. Considering that SSHI and SCE interface circuits have been proven to be more efficient than the standard interface circuit [19, 23] the standard interface circuit is not analyzed in detail in this paper. Although many improved interface circuits have been introduced in recent years [7, 8, 16] the interface circuit utilized in the simulation in this study is based on [13, 19, 23]. The self-powered parallel SSHI interface circuit is shown in Figure 7, with its component models or values in Table 1. The self-powered series SSHI interface circuit is shown in Fig. 8, with its component models or values in Table 2. The self-powered SCE interface circuit is shown in Fig. 9, with its component models or values

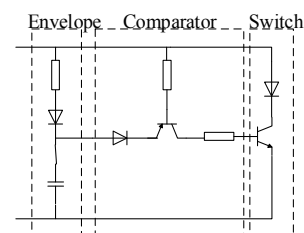


Figure 6: Electronic breaker for switch-on maximum displacement [19]

Table 1: Component models or values for parallel SSHI interface circuit

Component	Model/Value
R <sub>1</sub> , R <sub>6</sub>	510 KΩ
R <sub>2</sub> , R <sub>3</sub> , R <sub>4</sub> , R <sub>5</sub>	10 KΩ
C <sub>1</sub> , C <sub>2</sub>	4 nF
Diodes (D <sub>1</sub> to D <sub>10</sub> )	1N4004
PNP transistors (Q <sub>1</sub> and Q <sub>3</sub> )	TIP32C
NPN transistors (Q <sub>2</sub> and Q <sub>4</sub> )	TIP31C
C <sub>rect</sub>	10 μF
L	47 mH

Table 2: Component models or values for series SSHI interface circuit

Component	Model/Value
R <sub>1</sub> , R <sub>2</sub>	200 KΩ
C <sub>1</sub> , C <sub>2</sub>	2 nF
Diodes (D <sub>1</sub> to D <sub>8</sub> )	1N4004
PNP transistors (Q <sub>1</sub> and Q <sub>4</sub> )	TIP32C
NPN transistors (Q <sub>2</sub> and Q <sub>3</sub> )	TIP31C
C <sub>rect</sub>	10 μF
L	47 mH
r	178 Ω

in Table 3. For the standard interface circuit, the model of the diodes is 1N4004, and the capacitance value is 10 μF.

For a certain interface circuit in piezoelectric energy harvesting systems, the output power of different resistance values should be acquired first. Then, the parameters that influence the output power most should be identified. Finally, the selected parameters that influence the output power most should be optimized to ensure that the performance of the collecting circuit is improved. The circuit design flow is shown in Fig. 10. For each interface circuit, in the simulation environment using OrCAD 16.3, the circuit was set up by using Capture. Then, circuit simulation was performed when no errors exist in the circuit diagram. Transient and para-

metric analyses of the parameter  $R_{load}$  were conducted by using PSpice AD and Probe to obtain the relationship between load resistance and output power. The optimal resistance value can be studied if one exists in the circuit. Next, the optimal resistor was used in the circuit, and the maximum value of the power of  $R_{load}$ , which is considered the output power, was set as the measurement to be used in the sensitivity analysis. Sensitivity analysis was conducted to analyze the influence of the component value on the performance of the circuit and to compare the magnitude of the influence of different component values on circuit performance. Hence, the key components that influence circuit performance the most can be obtained through sensitivity analysis. Based on sensitivity analysis, the circuit can be improved by performing an optimizer analysis by optimizing the most sensitive component values.

Sensitivity can be expressed by absolute and relative sensitivity. Relative sensitivity  $S_N$  is given in Eq. (??).

$$S_N = \frac{\partial T}{\partial X} \times \frac{X}{100} \quad (8)$$

where:  $T$  represents a circuit performance parameter,  $X$  represents a component value, and  $\frac{\partial T}{\partial X}$  represents the absolute sensitivity. In our sensitivity analysis,  $T$  is the power of load resistance, and  $X$  is the value of a resistor or a capacitor in the circuit.

Optimization analysis was conducted by using the optimizer tool to set the constraints and by adjusting the parameters of components in the circuit constantly. Iteration of the circuit simulation will not be finished until the performance goal is reached. Thus, an optimization process involves many circuit simulations. In the process, adjusting the parameters, iterations, and result judgments is performed automatically with the modified least squares quadratic (MLSQ) engine.

#### 4. Results Analysis and Discussion

The harvested power was investigated under different situations. The value of  $I_p$  and  $C_p$  was tested or calculated with Eqs. (3), (4), (5), and (7), and the frequency was set to 2 Hz representing people walking.  $I_p$  and  $C_p$  were set to 200 μA and 100 nF, respectively.

The simulation results under the 2 Hz condition shown in Fig. 11 demonstrate that the four circuits with corresponding parameters have different performances under different resistance values. Different interface circuits can be used in different situations. The sensitivity

Table 3: Component models or values for SCE interface circuit

Component	Model/Value
R <sub>1</sub>	120 KΩ
R <sub>2</sub>	51 KΩ
R <sub>3</sub>	10 KΩ
C <sub>1</sub>	820 pF
C <sub>rect</sub>	10 μF
L <sub>1</sub> , L <sub>2</sub>	100 mF
Diodes (D <sub>1</sub> to D <sub>7</sub> )	1N4004
D <sub>8</sub>	UF4004

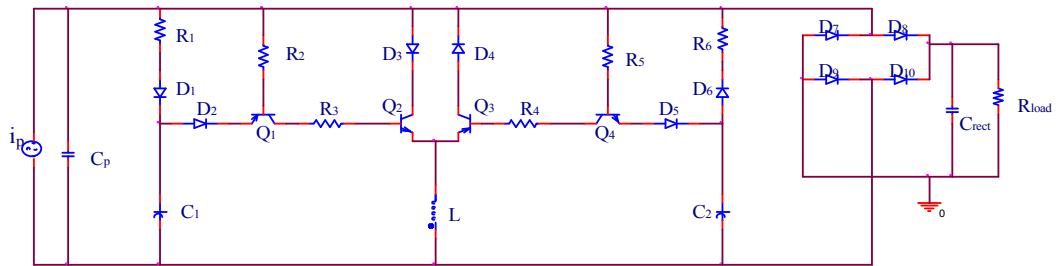


Figure 7: Self-powered parallel SSHI interface circuit [19]

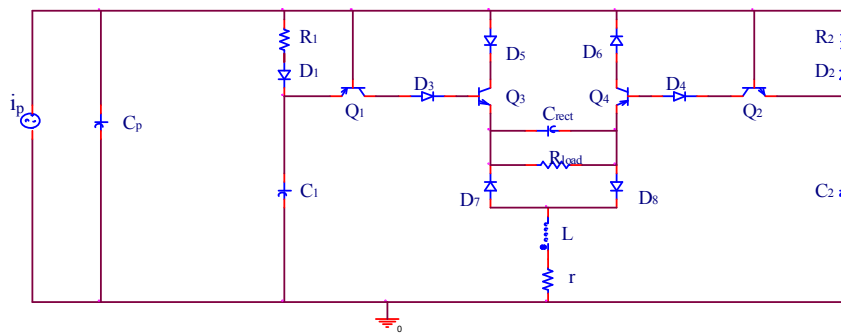


Figure 8: Self-powered series SSHI interface circuit[23]

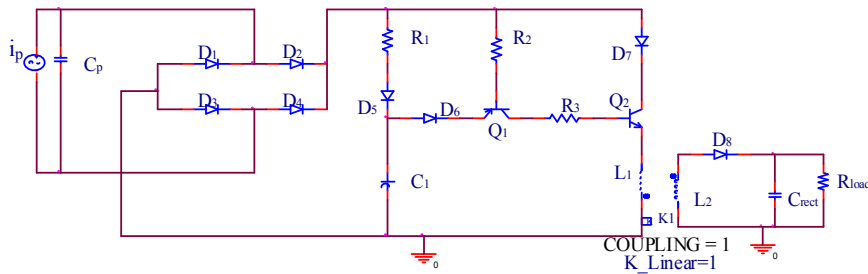


Figure 9: Self-powered SCE interface circuit [19]

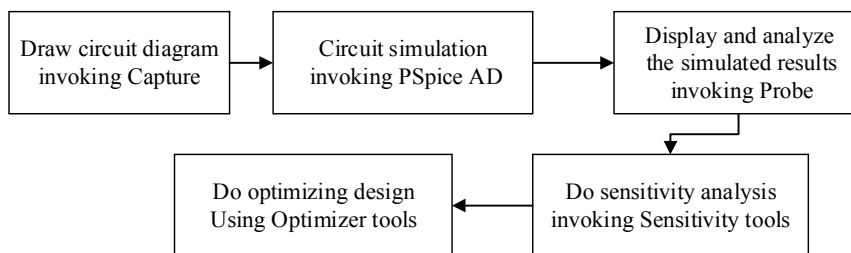


Figure 10: Circuit design flow

Table 4: Results of sensitivity analysis of P-SSHI circuit (2 Hz, 3,000 k)

Component	Relative sensitivity	Linear sensitivity comparison
C1	-57.89 u	98
C2	-16.03 u	27
R5	-7.00 u	11
R1	4.92 u	8
R4	-5.12 u	8
R2	-5.09 u	8
R6	-2.09 u	3
R3	-759.49 n	1

Table 5: Results of sensitivity analysis of S-SSHI circuit (2 Hz, 400 k)

Component	Relative sensitivity	Linear sensitivity comparison
r	-148.42u	91
C1	-55.25u	34
R1	-32.14u	19
C2	-28.43u	17
R2	17.36u	10
L	13.04u	8

analysis results of different interface circuits with different load resistance values are shown in Table 4, Table 5 and Table 6.

Through an optimizer analysis, the output power of the load resistor can be increased. For instance, the load output power of the SCE interface circuit with a resistance value of 10 KΩ can be optimized from 11.98 mW to 19.85 mW, and the load output power of the P-SSHI interface circuit with a resistance value of 3,000 KΩ can be optimized from 20.13 mW to 25.23 mW. The optimizing performance of the S-SSHI interface circuit is not good, which means the original parameters are good enough.

### 5. Conclusions

This study introduced an optimization method to improve the working performance of interface circuits

Table 6: Results of sensitivity analysis of SCE circuit (2 Hz, 10 k)

Component	Relative sensitivity	Linear sensitivity comparison
C1	562.98u	98
L1	220.04u	38
R2	-209.07u	36
L2	201.33u	35
R3	169.21u	29
R1	-10.34u	1

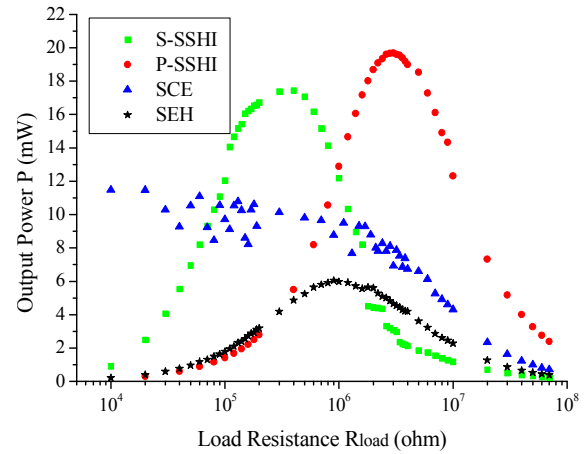


Figure 11: Harvested power versus load resistance (2 Hz)

in piezoelectric energy harvesting systems. Simulation analysis for optimization, which is a time-saving and cost-saving means of optimizing the collecting circuits, was conducted. A parametric analysis was performed to ensure that the circuit operates correctly. After the parametric analysis, a sensitivity analysis was conducted to determine the parameters that influence the performance goal the most. Through the sensitivity analysis, the parameters that influence the performance goal the most were selected as the optimizable parameters for the optimization analysis, which can increase the optimization speed. Specifications, including constraints and the performance goal, should be set in the optimization analysis. The main results are shown as follows:

1. The optimization method can be used effectively to optimize the load output power by setting the power as the performance goal. The output power is increased, and the parameters are changed automatically through iterations.
2. The constraints and performance goals should be set to proper values. If the value is not appropriate, the iterations will fail.

In the future, further analyses and experiments should be conducted to achieve significant progress.

### Acknowledgments

This work was supported by the National Natural Science Foundation of China (Grant No. 31170669).

## References

- [1] H. A. Sodano, D. J. Inman, G. Park, A review of power harvesting from vibration using piezoelectric materials, *Shock and Vibration Digest* 36 (3) (2004) 197–206.
- [2] S. R. Platt, S. Farritor, H. Haider, On low-frequency electric power generation with pzt ceramics, *Mechatronics, IEEE/ASME Transactions on* 10 (2) (2005) 240–252.
- [3] V. W. Mahyastuty, A. A. Pramudita, Low energy adaptive clustering hierarchy routing protocol for wireless sensor network, *TELKOMNIKA (Telecommunication Computing Electronics and Control)* 12 (4) (2014) 963–968.
- [4] C.-H. Chao, A remote power management strategy for the solar energy powered bicycle, *TELKOMNIKA (Telecommunication Computing Electronics and Control)* 9 (3) (2013) 483–488.
- [5] M. F. B. A. Rahman, S. L. Kok, Investigation of useful ambient vibration sources for the application of energy harvesting, in: *Research and Development (SCOReD)*, 2011 IEEE Student Conference on, IEEE, 2011, pp. 391–396.
- [6] E. Arroyo, A. Badel, F. Formosa, Y. Wu, J. Qiu, Comparison of electromagnetic and piezoelectric vibration energy harvesters: model and experiments, *Sensors and Actuators A: Physical* 183 (2012) 148–156.
- [7] L. Zhu, R. Chen, A new synchronized switching harvesting scheme employing current doubler rectifier, *Sensors and Actuators A: Physical* 174 (2012) 107–114.
- [8] Y. Wu, A. Badel, F. Formosa, W. Liu, A. Agbossou, Self-powered optimized synchronous electric charge extraction circuit for piezoelectric energy harvesting, *Journal of Intelligent Material Systems and Structures* 25 (17) (2014) 2165–2176.
- [9] F. Cottone, L. Gammaitoni, H. Vocca, M. Ferrari, V. Ferrari, Piezoelectric buckled beams for random vibration energy harvesting, *Smart materials and structures* 21 (3) (2012) 035021.
- [10] W. Liu, A. Badel, F. Formosa, Y. Wu, A. Agbossou, Novel piezoelectric bistable oscillator architecture for wideband vibration energy harvesting, *Smart materials and structures* 22 (3) (2013) 035013.
- [11] J. Qiu, H. Jiang, H. Ji, K. Zhu, Comparison between four piezoelectric energy harvesting circuits, *Frontiers of Mechanical Engineering in China* 4 (2) (2009) 153–159.
- [12] G. K. Ottman, H. F. Hofmann, A. C. Bhatt, G. A. Lesieutre, Adaptive piezoelectric energy harvesting circuit for wireless remote power supply, *Power Electronics, IEEE Transactions on* 17 (5) (2002) 669–676.
- [13] M. Lallart, É. Lefeuvre, C. Richard, D. Guyomar, Self-powered circuit for broadband, multimodal piezoelectric vibration control, *Sensors and Actuators A: Physical* 143 (2) (2008) 377–382.
- [14] I. Lien, Y. Shu, W. Wu, S. Shiu, H. Lin, Revisit of series-sshi with comparisons to other interfacing circuits in piezoelectric energy harvesting, *Smart Materials and Structures* 19 (12) (2010) 125009.
- [15] L. Tang, Y. Yang, Analysis of synchronized charge extraction for piezoelectric energy harvesting, *Smart Materials and Structures* 20 (8) (2011) 085022.
- [16] Y. Wu, A. Badel, F. Formosa, W. Liu, A. E. Agbossou, Piezoelectric vibration energy harvesting by optimized synchronous electric charge extraction, *Journal of Intelligent Material Systems and Structures* 24 (12) (2013) 1445–1458.
- [17] A. Badel, A. Benayad, E. Lefeuvre, L. Lebrun, C. Richard, D. Guyomar, Single crystals and nonlinear process for out-standing vibration-powered electrical generators, *IEEE transactions on ultrasonics, ferroelectrics, and frequency control* 53 (4) (2006) 673–684.
- [18] J. Liang, W.-H. Liao, Impedance modeling and analysis for piezoelectric energy harvesting systems, *Mechatronics, IEEE/ASME Transactions on* 17 (6) (2012) 1145–1157.
- [19] L. Zhu, R. Chen, X. Liu, Theoretical analyses of the electronic breaker switching method for nonlinear energy harvesting interfaces, *Journal of Intelligent Material Systems and Structures* 23 (4) (2012) 441–451.
- [20] J. Scruggs, An optimal stochastic control theory for distributed energy harvesting networks, *Journal of Sound and Vibration* 320 (4) (2009) 707–725.
- [21] J. Scruggs, On the causal power generation limit for a vibratory energy harvester in broadband stochastic response, *Journal of Intelligent Material Systems and Structures* 21 (13) (2010) 1249–1262.
- [22] J. Schoeftner, G. Buchberger, A contribution on the optimal design of a vibrating cantilever in a power harvesting application—optimization of piezoelectric layer distributions in combination with advanced harvesting circuits, *Engineering Structures* 53 (2013) 92–101.
- [23] J. Liang, W.-H. Liao, Improved design and analysis of self-powered synchronized switch interface circuit for piezoelectric energy harvesting systems, *Industrial Electronics, IEEE Transactions on* 59 (4) (2012) 1950–1960.